Quantifying Metrics for Wildfire Ignition Risk from Geographic Data in Power Shutoff Decision-Making

Abstract

To mitigate the threat of wildfire ignitions from electric power infrastructure, utilities preemptively de-energize power lines, which may result in power shutoffs. Data regarding wildfire ignition risks are key inputs for planning power line de-energizations. There are multiple ways to formulate risk metrics that spatially aggregate risk map data. Considering both threshold- and optimization-based methods for planning power line de-energizations, this paper defines and compares the results of employing six metrics for quantifying the wildfire ignition risks of power lines from risk maps. The numeric results use the California Test System (CATS), a large-scale synthetic grid model with power line paths accurate to the infrastructure in California. This is the first application of the optimal power shutoff on such a large and realistic test case. Using Wildland Fire Potential Index maps for an entire year, we show that the choice of risk metric significantly impacts the lines that are de-energized and resulting load shed.

Keywords: Optimization, power shutoff, wildfire ignition risk.

1. Introduction

Power systems operators are increasingly concerned with the potential for electrical faults to ignite wildfires. In addition to an aging electric grid, both organic material buildup due to decades of fire suppression and climate change are intensifying fire risk conditions. In California, land area burned due to wildfires is predicted to increase between 3% and 52% by 2050 based on a climate model ensemble [1]. Fires ignited from power equipment are common [2] and tend to burn more area than wildfires ignited from other sources [3], likely because high winds increase both fault probability and fire spread rate. Thus, operators face a complex environment in which they must avoid igniting wildfires while ensuring reliable access to electricity. To better inform line de-energization planning, this paper characterizes how differences in wildfire ignition risk quantification can impact decisions in power grid operations.

To mitigate the risk of wildfire ignitions from power lines, many utilities implement preemptive power shutoffs—called "Public Safety Power Shutoffs" (PSPSs)—which involve selectively de-energizing certain power lines (via switching) to eliminate the possibility of these lines igniting fires. While this is an effective fire risk reduction strategy, it concurrently can lead to customer outages. To prioritize risk mitigation actions, many utilities use threshold-based methods that de-energize lines whose associated risk values exceed a pre-determined threshold [4]. Researchers have proposed algorithms to better manage these trade-offs by considering both wildfire ignition risk and load shed due to power shutoffs when determining which lines to shut off. Reference [5] proposes an optimization model, referred to as the "Optimal Power Shutoff" (OPS) problem, to balance wildfire risk and load shed. Similar works and extensions are proposed for multi-period shutoff scheduling [6], [7], security-constrained optimal power flow [8], stochastic unit commitment [9], alternative mitigation actions such as dynamic line rating [10] and microgrid formation [11], power restoration [12], social equity considerations [13], and long-term investment planning [14]–[16]. Machine learning techniques have also been applied to predict ignitions from power lines [17] and to relate input wildfire scenarios and output mitigation strategies [18]. All of these models are sensitive to the specifics of

wildfire risk parameters. Therefore, it is important to carefully consider how wildfire risk metrics for individual power lines are formulated.

Consistent with the definitions in [19] and [20], we consider wildfire ignition risk from power lines in terms of two components: fault probability and wildfire potential. An electrical fault occurs when an abnormal event (e.g., contact with vegetation or animals, conductor clashing, and downed power lines) results in current flow outside of a power line conductor. These events might involve involve arcing, sparks, and burning equipment or vegetation. Fault probability is influenced by factors specific to power systems in addition to weather conditions (e.g., wind) and vegetation factors. The likelihood of a fault is a function of the age and condition of infrastructure, right-of-way, line loading and sagging, and voltage level. A fault leads to an energy release that can ignite a wildfire. Wildfire potential, on the other hand, captures an ignition's impact, i.e., the subsequent potential for fire spread and intensity. This potential is dependent on factors that are not specific to power systems but rather is due to weather and vegetation conditions in the region surrounding an ignition.

While many faults occur, the probability of a fault occurring at any particular time and place is small and difficult to assess. Reference [21] propose a risk metric that includes both fault probability and fire potential factors. Reference [22] analyzes fault probability due to conductor clashing, comparing the use of a nonlinear model of conductor vibrational physics under wind forces with machine learning methods for fault prediction. Among other data requirements, these studies require information about distances between conductors and vegetation, the ground, and other conductors, which is not commonly available in models of real or synthetic power systems. Even utilities may not have this data, as line inspections are costly and time-consuming. Thus, consistent with much of the literature on wildfire risk mitigation, we assume in this paper that the probability of a fault occurring is constant throughout the power system and define wildfire ignition risk based on wildfire potential only.

Numerous approaches are available to quantify wildfire potential, leveraging a combination of surface meteorological measurements and satellite data. This includes "Fire Weather Watch" and "Red Flag Warning" areas [23], Significant Fire Potential Outlooks [24], and the Wildland Fire Potential Index (WFPI) [25]. Other tools simulate fire spread, such as FSim [26] and FlamMap [27]. Another tool, Pyrecast, aggregates fire simulation results from millions of simulated ignition points to produce static maps of burned area risk [28].

We leverage the availability of high-fidelity wildfire risk maps to characterize the risk of energized lines. WFPI and Pyrecast risk maps are good candidates for quantifying wildfire ignition risk from power equipment failure because of their temporal granularity (published daily and hourly, respectively), fine spatial granularity (1 square kilometer and 30 square meters, respectively) and the use of a range of potential levels (indices from 0 to 247 and the number of times each land area "pixel" is burned in the Monte Carlo sample set, respectively) rather than a binary "threat" categorization. Researchers commonly overlay geospatial grid data on top of such risk maps to obtain wildfire ignition risk values for individual power lines. Fig. 1 shows the CATS transmission lines paths superimposed on a WFPI map.

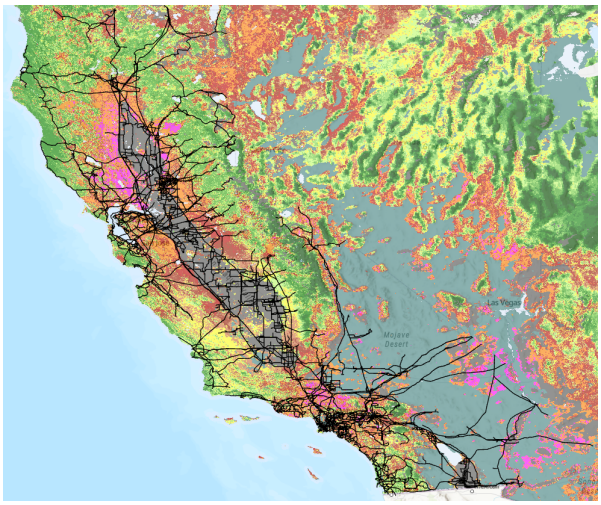

Figure 1. California Test System lines superimposed on a Wildland Fire Potential Index Map for October 26, 2020.

Clearly, power lines will generally intersect multiple wildfire potential values, thus raising the question of how to appropriately aggregate risk values along the length of the line. Past works have opted to use the maximum intersecting risk value [9], [11], [12], [19] or a sum of intersecting risk values [13], [14], [29] for aggregation. However, it is not clear whether the maximum value accurately captures the risk of the entire line, as two lines with the same point-wise maximum value may have different risk at other points; a decision-maker may be interested in prioritizing mitigation for the line with high risk along a significant fraction of the line. Cumulative metrics, on the other hand, may not capture points of extreme risk, as the maximum value would. This motivates alternate strategies of aggregating risk such as computing the mean or thresholding out low intersecting risk values.

A comparison of maximum and cumulative wildfire risk metrics in [19] demonstrates that varying choices of risk metric produce significantly different optimal capital investments for long-term wildfire risk mitigation. However, the analysis in [19] has several limitations: mean wildfire risk metrics are not considered, the optimal investment model does not include a power flow representation, and the test network (the RTS-GMLC case [30]) is relatively small and does not have realistic power line paths.

This paper addresses these limitations while also analyzing additional risk metrics. We compare the performance of these metrics considering two methods for determining line de-energizations to limit the wildfire ignition risk in a power system: (1) a threshold-based approach and (2) an optimal power shutoff problem. We demonstrate results on the California Test System [31], a 9000-bus synthetic test system with line paths that accurately represent the actual transmission system in California.

Our primary contributions are as follows:

- We apply threshold- and optimization-based power shutoff plans to the California Test System, a synthetic grid model with power line paths accurate to the actual infrastructure in California. This is the first application of the optimal power shutoff problem to such a large and realistic test case in the academic literature.
- We compare the impacts of different wildfire risk aggregation metrics on the resulting shutoff plans.
- We find that metrics based on the normal risk data result in significant differences among de-energization plans, while using post-processed risk data yields much smaller variation in the results obtained by different metrics.
- We find the that the optimization-based power shut off method results in an approximately 80% reduction of the load shed compared to the threshold-based method while maintaining the same overall wildfire ignition risk.

The remainder of the paper is organized as follows. Section 2 introduces the six risk metrics we consider. Section 3 details the methods for planning power grid shutoffs. Section 4 describes our case study and presents computational results. Section 5 concludes the paper.

2. Wildfire Risk Metrics

We define six metrics that quantify the wildfire ignition risk of individual power lines derived from existing wildfire risk maps. We use the WFPI map from the U.S. Geological Survey [25]. The WFPI is a measure of vegetation flammability and represents the relative potential for large fires and fire spread in a particular location. The index is calculated at a spatial granularity of one square kilometer with a nominal range of 0-150. The index is enhanced by wind-speed, and can exceed 150 with very high wind speeds. This index is published daily to update the value associated with each 1 km by 1 km "pixel". Some land types such as desert and marshland do not have an index associated with them because they are considered "un-burnable". Agricultural land also does not have a risk value because the vegetation type and moisture levels are constantly changing and not available for calculating the wildfire risk.

The wildfire risk metric for a power line is derived from the pixels of a wildfire risk map that a power line intersects. Lines typically cross many 1 km grid squares with potentially high variance in risk values, as shown in Fig. 1. Grid operators want to mitigate the risk of lines igniting fires, but are not able to de-energize just the high-risk segments of power lines. To assess the need for de-energization, we must aggregate the risk values that a power line passes through to obtain a metric for the entire line. Our primary objective is to analyze how the choice of risk aggregation metric impacts decision-making in power grid operations involving line de-energization.

We next define six power line wildfire risk metrics. The first three metrics are based on the mean, maximum, and cumulative values of the pixels the power lines traverse, respectively. The last three metrics use an additional pre-processing step to only consider the pixels whose risk values are above a particular threshold.

2.1. Baseline Wildfire Risk Metrics

For a power line ℓ, let $\mathcal{P}_\ell$ denote the set of pixel indices p that the power line intersects. Let $\mathcal{R}_{\ell dp}$ denote the set of pixel risk values on day d for line ℓ. For each line and on each day, we aggregate these values as the maximum, mean, or cumulative value. The formal definitions for each metric are provided below, along with discussions of their characteristics.

Maximum (MA) Metric The maximum metric (MA) assigns a risk value for each line equivalent to the maximum risk of any pixel that the line intersects:

$$R^{MA}_{\ell d} = \max_{p \in \mathcal{P}_\ell} R_{\ell dp}. \tag{1}$$

Selecting the maximum risk value directly emphasizes the worst-case risk of a wildfire ignition along a corridor.

This metric ignores the length of a power line, and therefore how many pixels it traverses and the variance of those risk values. For instance, a 1 km line crossing a single high-risk pixel is treated the same as a 10 km line crossing ten high-risk pixels and the same as a 300 km line crossing a single high-risk pixel and 299 low-risk pixels.

Mean (ME) Metric The mean metric (ME) assigns a risk value that is the average of the pixels that the line intersects:

$$R_{\ell d}^{ME} = \frac{\sum_{p \in \mathcal{P}_\ell} R_{\ell dp}}{|\mathcal{P}_\ell|}. \tag{2}$$

Averaging risk values helps to identify lines that have a greater proportion of their lengths in high-risk areas. For example, a 10 km line with a 9 km segment in a high-risk region is given a higher risk than a 10 km line with 1 km in high-risk regions, but it is also higher risk than a 100 km line with 20 km in high-risk regions. This metric also does not capture the length of the power line as a factor that increases the risk.

Cumulative (CU) Metric The cumulative metric (ME) assigns a risk that is the sum of the pixels that the line intersects:

$$R_{\ell d}^{CU} = \sum_{p \in \mathcal{P}_\ell} R_{\ell dp}. \tag{3}$$

The cumulative metric sums all of the risk values along the length of the power line. This captures the intuitive sense that a 100 km line is more likely to start a fire somewhere than a 1 km line, but the metric for a long line can dominate the cumulative risk of a short line with a larger individual risk value. For example, a 10 km line with 5 km in high-risk regions could have a lower R^{CU} value than a 100 km line with the entire length in low-risk regions.

2.2. Pre-Processing Wildfire Risk

We now describe a method of pre-processing wildfire risk data to better identify the highest risk pixels before aggregating the risk values into a metric. This method, adapted from [29], uses a risk threshold, where pixel p is removed from the set if the risk $R_{\ell dp}$ is below the threshold. The purpose of this processing is to ignore sections of lines where the risk is low, and only keep pixel risk values that are above this threshold.[1]

[1]We note that this pre-processing threshold is a separate threshold from the threshold-based method discussed in Section 3.1 for selecting which lines to de-energize.

To compute the threshold value, we consider the annual wildfire risk values of a previous year. We take the set of all risk values $\mathcal{R}_{\ell dp}$ for all lines $\ell \in \mathcal{L}$, for all days $d \in D$, and for all pixel indices $p \in \mathcal{P}_\ell$. We find the average risk value $\bar{r}$ and the standard deviation of risk values σ of this set. We define our threshold of interest as any risk value greater than one standard deviation above the mean. The set of pixels above the threshold for each line on each day is defined as

$$P_{\ell d}^h = \{p \in P | R_{\ell,d,p} \geq \bar{r} + \sigma\}, \quad \forall \ell \in \mathcal{L}, \forall d \in D. \tag{4}$$

We define this new set of pixels rather than set the risk metric to zero for pixels below the threshold to better capture the intent of the mean risk metric defined below. With this definition, we will only average the high-risk pixels rather than include many zero values when calculating the average. We next introduce the aggregation metrics with the high-risk thresholded risk values and discuss how these metrics alter the incentives from the normal risk values.

High-Risk Maximum (HRMA) Metric The high-risk maximum metric (HRMA) assigns a risk value equal to the maximum risk a line intersects in the high-risk pixel set:

$$R_{\ell d}^{MA} = \max_{p \in P_{\ell d}^{HR}} R_{\ell dp}. \tag{5}$$

This high-risk maximum risk metric is the same as the baseline for any line that has a risk value above the risk threshold. For any line whose maximum risk is below the risk threshold, the maximum value is zero rather than its baseline value. This removes any incentive to de-energize low- or moderate-risk power lines.

High-Risk Mean (HRME) Metric The high-risk mean metric (HRME) assigns a risk value equal to the mean of the high-risk pixels that a line intersects:

$$R_{\ell d}^{ME} = \frac{\sum_{p \in P_{\ell d}^{HR}} R_{\ell dp}}{|P_{\ell d}^{HR}|}. \tag{6}$$

The high-risk mean metric only averages the values above the threshold. For this metric, a 10 km line with 5 km in high-risk regions would have the same risk as a 100 km line with 5 km in high-risk regions. Compared to the baseline mean metric, this metric removes the "penalty" to risk values that occurs for long lines with large sections in low-risk regions.

High-Risk Cumulative (HRCU) Metric The high-risk cumulative metric (HRCU) assigns a risk value equal to the sum of the high risk pixels that a line intersects:

$$R^{CU}_{\ell d} = \sum_{p \in P^{HR}_{\ell d}} R_{\ell dp}. \tag{7}$$

The high-risk cumulative metric sums all risk values above the threshold. Under this metric, a long line through a low-risk region will not be assigned a high risk value, but lines with long stretches through high-risk regions will still have higher risk values compared to short lines through these regions.

2.3. Risk Metric Summary

We define six risk metrics to summarize the wildfire risk along a power line: MA, ME, CU, HRMA, HRME, and HRCU. Each of these metrics provide a different incentive for a de-energization strategy, from prioritizing the longest power lines to prioritizing the highest risk segment of a line no matter the length. In the modeling efforts below, we incorporate these metrics to show their impacts on Public Safety Power Shutoff de-energization plans.

3. Power Shutoff Decision-Making

Given risk values for all lines in a power system, an operator can make a decision concerning which lines should be de-energized in order to decrease the overall potential for power infrastructure to ignite wildfires. This work assesses two common analytic methods for determining how to implement power shutoffs: thresholding and optimal power shutoffs.

3.1. Thresholding

One mitigation option is to de-energize any line that is considered "risky", i.e., any line that has a risk value that exceeds some predetermined level or threshold. This approach requires selection of a risk threshold that is not too high so that we do not fail to turn off lines that are likely to ignite dangerous fires, but that is not too low such that numerous lines are de-energized with associated customer outages.

We choose a threshold using statistical measures, specifically the 95^{th}-percentile of risk values (across all lines and all scenarios) for a particular metric. In other words, we consider the risk associated with each line-day pair. We then select the pairs with risks in the 95^{th}-percentile and de-energize these lines on the associated days. This results in lines being *aggressively* de-energized, one to two orders of magnitude more than seen historically, resulting in large quantities of load shed. This provides the optimal power shutoff problem (see Section 3.2) with a large amount of wildfire risk to remove through de-energization decisions, resulting in non-zero load shed even in the optimal cases.

One way to evaluate the suitability of a particular threshold is to examine the extent and frequency of historical power shutoffs for comparison with the extent and frequency of shutoffs that result from a particular threshold. The California Public Utilities Commission (CPUC) requires that electric utilities in California report information about wildfire events and public safety power shutoffs that they implement. The large investor-owned utilities Pacific Gas & Electric (PG&E), Southern California Edison (SCE), and San Diego Gas & Electric (SDG&E) publish reports on their websites [32]–[34] and the CPUC aggregates that data in their "PSPS Event Rollup Report" [35]. In 2023, PG&E included the line-miles of transmission/distribution de-energized in their reporting (which would be helpful for assessing PSPS extent), but the company only reported two PSPS events for the year 2023, as this was a relatively unsevere wildfire season. In 2020 and 2021, there were 31 and 16 unique days, respectively, during which a PSPS "Outage Start" occurred. The threshold chosen for this paper results in many more PSPS events.

A shortcoming of the thresholding approach is that it does not consider the load-serving potential of power lines. This motivates the optimal power shutoff approach.

3.2. Optimal Power Shutoff

The optimal power shutoff (OPS) problem is a grid optimization problem that determines steady-state grid operations decisions (including generator output, line flow, load served, and bus voltage angles) as well as binary line de-energization decisions in a way that balances wildfire risk mitigation with load that is shed due to those de-energizations. The OPS is first proposed in [5]. The following works study and extend the OPS [6]–[16], [29].

There are several ways to formulate the risk and load shed mitigation strategies in the OPS problem. For example, we can formulate a multi-objective problem that minimizes wildfire risk and load shed, as in [5], [13], [14], or we can minimize wildfire risk while constraining load shed to some acceptable level as in [8] (or vice versa as in [29]). For this paper, since we are interested in comparing metrics for wildfire risk, we choose to minimize load shed while constraining wildfire risk. This allows us to maintain a safe level of wildfire ignition risk in the network while optimizing

Model 1 Optimal Power Shutoff (OPS)

$$\textbf{min} \sum_{t\in\mathcal{T}}\sum_{n\in\mathcal{N}} p^n_{ls,t} + \epsilon_{\text{switch}} \sum_{\ell\in\mathcal{L}^{\text{switch}}} z^\ell \tag{8a}$$

s.t. $\forall t \in \mathcal{T}$,

$$\underline{p}^i_g \leqslant p^i_{g,t} \leqslant \overline{p}^i_g \qquad \forall i \in \mathcal{G} \tag{8b}$$

$$0 \leqslant p^n_{ls,t} \leqslant p^n_{d,t} \qquad \forall n \in \mathcal{N} \tag{8c}$$

$$-\overline{f}^\ell z^\ell \leqslant f^\ell_t \leqslant \overline{f}^\ell z^\ell \qquad \forall \ell \in \mathcal{L}^{\text{switch}} \tag{8d}$$

$$-\overline{f}^\ell \leqslant f^\ell_t \leqslant \overline{f}^\ell \qquad \forall \ell \in \mathcal{L}\setminus\mathcal{L}^{\text{switch}} \tag{8e}$$

$$\theta^{n^{\ell,\text{fr}}}_t - \theta^{n^{\ell,\text{to}}}_t \geqslant \underline{\delta}^\ell z^\ell + \underline{M}(1-z^\ell) \qquad \forall \ell \in \mathcal{L}^{\text{switch}} \tag{8f}$$

$$\theta^{n^{\ell,\text{fr}}}_t - \theta^{n^{\ell,\text{to}}}_t \leqslant \overline{\delta}^\ell z^\ell + \overline{M}(1-z^\ell) \qquad \forall \ell \in \mathcal{L}^{\text{switch}} \tag{8g}$$

$$\underline{\delta}^\ell \leqslant \theta^{n^{\ell,\text{fr}}}_t - \theta^{n^{\ell,\text{to}}}_t \leqslant \overline{\delta}^\ell \qquad \forall \ell \in \mathcal{L}\setminus\mathcal{L}^{\text{switch}} \tag{8h}$$

$$f^\ell_t \geqslant -b^\ell(\theta^{n^{\ell,\text{fr}}}_t - \theta^{n^{\ell,\text{to}}}_t) + |b^\ell|\underline{M}(1-z^\ell) \;\forall \ell \in \mathcal{L}^{\text{switch}} \tag{8i}$$

$$f^\ell_t \leqslant -b^\ell(\theta^{n^{\ell,\text{fr}}}_t - \theta^{n^{\ell,\text{to}}}_t) + |b^\ell|\overline{M}(1-z^\ell) \;\forall \ell \in \mathcal{L}^{\text{switch}} \tag{8j}$$

$$f^\ell_t \geqslant -b^\ell(\theta^{n^{\ell,\text{fr}}}_t - \theta^{n^{\ell,\text{to}}}_t) \qquad \forall \ell \in \mathcal{L}\setminus\mathcal{L}^{\text{switch}} \tag{8k}$$

$$f^\ell_t \leqslant -b^\ell(\theta^{n^{\ell,\text{fr}}}_t - \theta^{n^{\ell,\text{to}}}_t) \qquad \forall \ell \in \mathcal{L}\setminus\mathcal{L}^{\text{switch}} \tag{8l}$$

$$\sum_{\ell\in\mathcal{L}^{n,\text{fr}}} f^\ell_t - \sum_{\ell\in\mathcal{L}^{n,\text{to}}} f^\ell_t = \sum_{i\in\mathcal{G}^n} p^i_{g,t} - p^n_{d,t} + p^n_{ls,t} \;\; \forall n \in \mathcal{N}. \tag{8m}$$

to reduce negative impact on loads compared to the thresholded baseline discussed in Section 3.1. The OPS formulation is outlined in Model 1.

Equation (8b) enforces lower ($\underline{p}^i_g$) and upper ($\overline{p}^i_g$) generation limits for power generation ($p^i_{g,t}$) at all generators $i \in \mathcal{G}$ at all times $t \in \mathcal{T}$. Equation (8c) constrains any load shedding ($p^n_{ls,t}$) to be nonnegative and less than the power demand ($p^n_{d,t}$) at that time at each bus $n \in \mathcal{N}$. Equations (8d) and (8e) enforce line flow (f^ℓ_t) to be within lower and upper limits ($\overline{f}^\ell$) in accordance with the energization status, z^ℓ, for lines $\ell \in \mathcal{L}$. For lines not in the switchable set $\mathcal{L}^{\text{switch}}$, note that z^ℓ is required to be set to one (indicating that the line is energized) instead of being a binary decision variable, thus reducing (8d) to (8e). Lines with zero risk are excluded from the switchable set $\mathcal{L}^{\text{switch}}$.

Equations (8f), (8g), and (8h) constrain the difference in voltage angle across a line ℓ from the from-bus $n^{\ell,fr}$ to the to-bus $n^{\ell,to}$ at each time step to be within the lower ($\underline{\delta}^\ell$) and upper ($\overline{\delta}^\ell$) limits in accordance with the line energization status. Again, if a line is not considered switchable, the energization status z^ℓ is set to one, thus reducing (8f) and (8g) to (8h).

Equations (8i), (8j), (8k), and (8l) model the DC power flow approximation with line energization status. Equations (8f), (8g), (8i), and (8j) utilize big-M constants to allow for voltage angle differences to be unconstrained across de-energized lines, with $\overline{M}$ and $\underline{M}$ set to 2π and -2π respectively for results shown in this paper. Note that more sophisticated methods for selecting big-M can be used, such as those in [36]. Equation (8m) ensures power balance at all buses in the network. The objective (8a) minimizes total load shed in the network with an associated penalty term on the number of de-energized lines. For then numerical results included in this paper, ϵ_{switch} is set to 0.01 to avoid the line switching decisions dominating the objective.

4. Test Case Results

We compare the performance of the six wildfire metrics and two shutoff methods utilizing the California Test System (CATS) [31]. CATS is a 9000-bus, 11000-line test system with transmission line paths that are based on actual grid infrastructure in California, but with synthetic parameters and topology so as not to reveal any critical information about the real grid. The geographic realism and large scale of CATS make it a compelling test case. However, it is important to note that the results derived here are not necessarily an indication of how California's actual power grid operates. We use the 2019 USGS WFPI daily risk data to determine high-risk pixel thresholds, and study de-energization plans on the 2020 wildfire risk data.

Computations are performed on the Partnership for an Advanced Computing Environment (PACE) at the Georgia Institute of Technology [37]. All models were implemented using Julia 1.9.2 [38] with PowerModels.jl v0.19.8 [39], and solved using Gurobi 10.0.1 [40].

To reduce solve times (due to the scale of the CATS system), we take a number of approaches. First, when finding optimal switching decisions, we warm-start the binary variables in the problem with the status of lines de-energized under the corresponding thresholded case. We also reduce the number of binary variables by only allowing lines with non-zero wildfire risk to be included in the switchable line set, $\mathcal{L}^{\text{switch}}$. We also relax the lower bound of generators to be 0 p.u. to avoid binary decision variables associated with generator on/off statuses. Finally, to reduce the size of the problem, we make switching decisions for the worst-case hour of the day, defined as the hour that had the most resulting load shed from the same day with lines de-energized subject to a given metric. After optimal line switching decisions are made on the given hour, these decisions are set for the full 24-hour period and hourly load shed and operational decisions are

found for the full day.

4.1. De-energization Decisions with Thresholding

Thresholding decisions differ between the normal and high-risk methodology. As can be seen in Figure 2, each method provides different line de-energization outcomes throughout the year. Both the CU and HRCU see a more uniform number of de-energized lines throughout the year while MA, ME, HRMA, and HRME all see more variation in numbers of de-energized lines. Figure 2 also shows that the the number of de-energized lines resulting from metrics with the high-risk pixel threshold (HRMA, HRME, HRCU) are more closely aligned throughout the year than those from the metrics which use the raw wildfire data (MA, ME, CU).

The first row of Table 1 shows the number of unique lines de-energized by the thresholded method at any time during 2020. We note that while the MA and ME metrics de-energize the same or nearly the same number of unique lines as the HRMA and HRME metrics, the HRCU metric de-energizes nearly double the number of unique lines over the span of the year. The resulting load shed on each day for each metric is shown in Figure 3. It is interesting to note that while the HRCU method de-energizes fewer lines than some other method, it results in the largest amount of load shed throughout the year. We also note that the MA and HRMA metrics de-energize the same number of unique lines (and the most by the thresholding method) but result in less load shed compared to other metrics for most of the year.

4.2. De-energization Decisions with OPS

When looking at the number of optimally de-energized lines in Figure 4, we see that the overall quantity of lines being de-energized is similar to the thresholded method. However, the optimal case de-energizes slightly more lines across all metrics. This is likely due to more lower-risk lines being de-energized to allow energization of some high-risk lines that are crucial for power delivery. By strategically de-energizing more low-risk lines, the overall risk in the network can be maintained while reducing the amount of load shed. Figure 5 shows that the optimal line switching decisions achieve approximately 20% of the load shed resulting from the thresholded method. Similar to the thresholded method, we again see that the CU and HRCU methods, while de-energizing fewer lines, result in larger amounts of load shed.

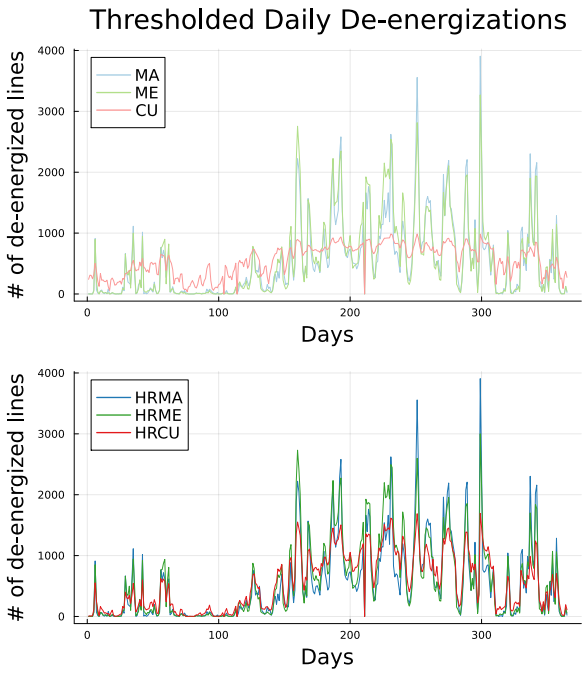

Figure 2. The number of lines de-energized on each day, by metric under the 95th-percentile thresholding method.

4.3. Comparing Thresholding and Optimal Decisions

While both thresholded and optimal de-energization decisions result in a similar number of lines being switched off, they do not select the same lines to be turned off throughout the year. Figure 6 shows the similarity between decisions made by each method/metric pairing. For each method/metric pair, we sum the number of times each individual line is de-energized. We then normalize each of these vectors and take the dot product. Thus, a value of 1.0 in the heat map indicates that line 1 was de-energized the same number of times throughout the year by both method/metrics, as was line 2, etc.

Figure 6 shows that thresholded MA and HRMA metrics produce the same results, and that the optimal MA and HRMA metrics produce nearly identical results. We also see that the decisions made by the ME or HRME metrics have very weak correlations with those made by the CU or HRCU metrics. Also note that the CU and HRCU metrics result in dissimilar decisions. This might be caused by the HRCU method de-energizing nearly double the number of lines compared to the CU method (as shown in Table 1).

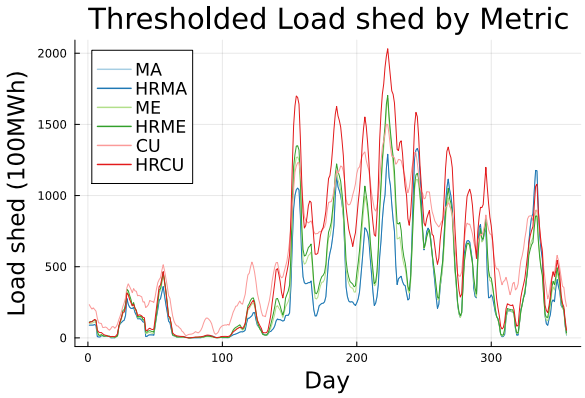

Figure 3. Seven-day rolling average load shed from thresholded line de-energization decisions.

	MA	HRMA	ME	HRME	CU	HRCU
Threshold	6376	6376	5204	5005	1206	2505
OPS	6307	6358	5555	5813	2917	5072

Table 1. The number of unique lines de-energized throughout 2020 for each metric in both the threshold and optimal power shutoff decisions.

5. Conclusions

This paper has characterized the impacts of different approaches to aggregating wildfire ignition risk data for power lines using a realistic large-scale synthetic power system. We defined and compared six different wildfire risk aggregation metrics using two different methods, thresholding and the optimal power shutoff, for making line de-energization decisions. The numerical results clearly show that the choice of metric significantly alters the de-energization decisions and associated load shed. Compared to thresholding, the optimal power shutoff formulation drastically reduces load shed (in a realistic large-scale network), despite a similar extent of line de-energizations and similar overall network risk.

Our future work will look at comparing modeled de-energization decisions with those made historically. In addition, extending our analysis to consider alternative modeling formulations would be valuable, such as a security-constrained optimal power shutoff, AC optimal power shutoff, and multi-period optimization.

Acknowledgements

The authors would like to thank Gurobi for providing the use of academic licenses for this work.

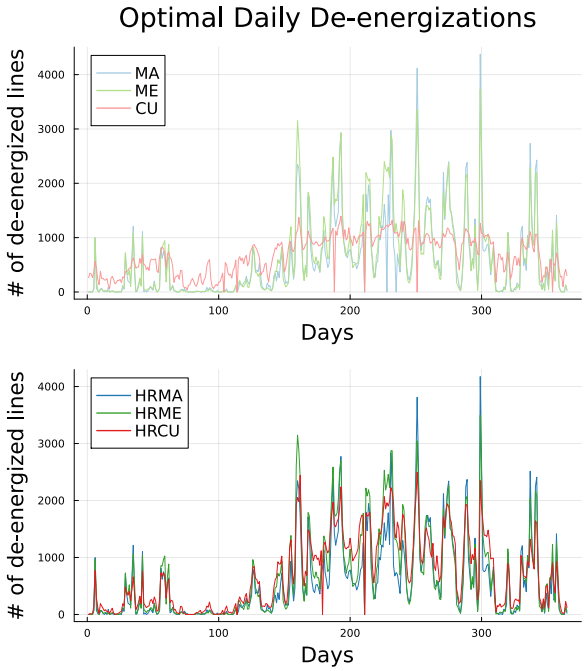

Figure 4. The number of lines de-energized on each day, by metric from optimal decisions for load shed minimization.

References

[1] M. Turco, J. T. Abatzoglou, S. Herrera, *et al.*, "Anthropogenic climate change impacts exacerbate summer forest fires in California," *Proceedings of the National Academy of Sciences*, vol. 120, 2023.

[2] California Public Utilities Commission, *Fire ignition data*, 2023. [Online]. Available: `https://www.cpuc.ca.gov/industries-and-topics/wildfires`.

[3] A. D. Syphard and J. E. Keeley, "Location, timing and extent of wildfire vary by cause of ignition," *International Journal of Wildland Fire*, vol. 24, no. 1, pp. 37–47, 2015.

[4] C. Huang, Q. Hu, L. Sang, *et al.*, "A review of public safety power shutoffs (PSPS) for wildfire mitigation: Policies, practices, models and data sources," *IEEE Transactions on Energy Markets, Policy and Regulation*, vol. 1, no. 3, pp. 187–197, 2023.

[5] N. Rhodes, L. Ntaimo, and L. Roald, "Balancing wildfire risk and power outages through optimized power shut-offs," *IEEE Transactions on Power Systems*, vol. 36, no. 4, pp. 3118–3128, 2021.

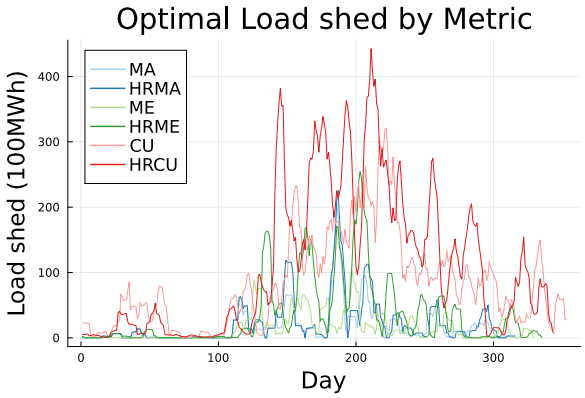

Figure 5. Seven-day rolling average load shed from optimal power shutoff line de-energization decisions.

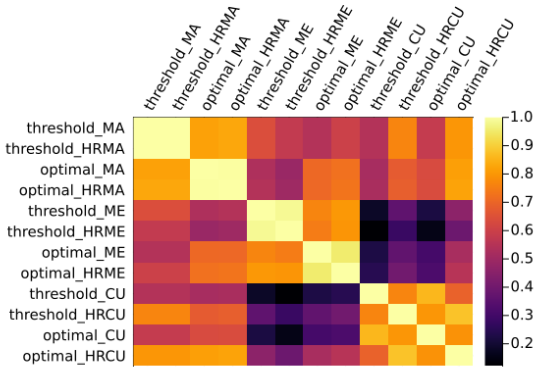

Figure 6. This heatmap shows how similar the line de-energization decisions are between the thresholded method and optimal methods with each metric over the full year. A value of 1.0 (yellow) indicates each line was de-energized the same number of times over the year while a value of 0.0 (black) indicates none of the same lines were de-energized over the year.

[6] A. Astudillo, B. Cui, and A. S. Zamzam, "Managing power systems-induced wildfire risks using optimal scheduled shutoffs," in *IEEE Power & Energy Society General Meeting (PESGM)*, 2022.

[7] A. Lesage-Landry, F. Pellerin, D. Callaway, and J. Taylor, "Optimally scheduling public safety power shutoffs," *Stochastic Systems*, vol. 13, no. 4, pp. 438–456, Jun. 2023.

[8] N. Rhodes, C. Coffrin, and L. Roald, "Security constrained optimal power shutoff," 2023. arXiv: 2304.13778.

[9] R. Greenough, K. Murakami, M. Davidson, J. Kleissl, and A. Khurram, *Wildfire resilient unit commitment under uncertain demand*, 2024. arXiv: 2403.09903.

[10] S. Tandon, S. Grijalva, and D. K. Molzahn, "Dynamic line rating and power flow control for wildfire mitigation," in *Power and Energy Conference at Illinois (PECI)*, Apr. 2021.

[11] S. Taylor, G. Setyawan, B. Cui, A. Zamzam, and L. A. Roald, "Managing wildfire risk and promoting equity through optimal configuration of networked microgrids," in *14th ACM International Conference on Future Energy Systems (ACM e-Energy 2023)*, Jun. 2023, pp. 189–199.

[12] N. Rhodes and L. A. Roald, "Co-optimization of power line shutoff and restoration under high wildfire ignition risk," in *IEEE Belgrade PowerTech*, 2023.

[13] A. Kody, A. West, and D. K. Molzahn, "Sharing the load: Considering fairness in de-energization scheduling to mitigate wildfire ignition risk using rolling optimization," in *61st IEEE Control and Decision Conference (CDC)*, Dec. 2022.

[14] A. Kody, R. Pianksy, and D. K. Molzahn, "Optimizing transmission infrastructure investments to support line de-energization for mitigating wildfire ignition risk," *11th Bulk Power Systems Dynamics and Control Symposium (IREP 2022)*, Jul. 2022.

[15] R. Bayani and S. D. Manshadi, "Resilient expansion planning of electricity grid under prolonged wildfire risk," *IEEE Transactions on Smart Grid*, vol. 14, no. 5, pp. 3719–3731, 2023.

[16] R. Piansky, G. Stinchfield, A. Kody, D. K. Molzahn, and J. P. Watson, "Long duration battery sizing, siting, and operation under wildfire risk using progressive hedging," to appear in *Electric Power Systems Research,* presented at the *23rd Power Systems Computation Conference (PSCC)*, 2024.

[17] M. Yao, M. Bharadwaj, Z. Zhang, B. Jin, and D. S. Callaway, "Predicting electricity infrastructure induced wildfire risk in California," *Environmental Research Letters*, vol. 17, no. 9, p. 094 035, Sep. 2022.

[18] W. Hong, B. Wang, M. Yao, D. Callaway, L. Dale, and C. Huang, "Data-driven power system optimal decision making strategy under wildfire events," in *55th Hawaii International Conference on System Sciences (HICSS)*, Jan. 2022.

[19] S. Taylor and L. A. Roald, "A framework for risk assessment and optimal line upgrade selection to mitigate wildfire risk," *Electric Power Systems Research*, vol. 213, p. 108 592, 2022, presented at the *22nd Power Systems Computation Conference (PSCC 2022)*.

[20] J. Su, S. Mehrani, P. Dehghanian, and M. A. Lejeune, "Quasi second-order stochastic dominance model for balancing wildfire risks and power outages due to proactive public safety de-energizations," *IEEE Transactions on Power Systems*, vol. 39, no. 2, pp. 2528–2542, 2024.

[21] N. Panossian and T. Elgindy, "Power system wildfire risks and potential solutions: A literature review & proposed metric," *National Renewable Energy Laboratory (NREL), technical report*, 2023.

[22] R. Bayani, M. Waseem, S. D. Manshadi, and H. Davani, "Quantifying the risk of wildfire ignition by power lines under extreme weather conditions," *IEEE Systems Journal*, vol. 17, no. 1, pp. 1024–1034, 2023.

[23] National Weather Service, *Fire Weather Hazard/Overview Map*, Jun. 2024. [Online]. Available: www.weather.gov/fire.

[24] National Interagency Fire Center, *Outlooks*, Jun. 2024. [Online]. Available: www.nifc.gov/nicc/predictive-services/outlooks.

[25] United States Geological Survey, *Wildland Fire Potential Index*, Jun. 2024.

[26] M. A. Finney, C. W. McHugh, I. C. Grenfell, K. L. Riley, and K. C. Short, "A simulation of probabilistic wildfire risk components for the continental United States," *Stochastic Environmental Research and Risk Assessment*, vol. 25, pp. 973–1000, 2011.

[27] M. A. Finney, "An overview of FlamMap fire modeling capabilities," in *Fuels Management–How to Measure Success: Conference Proceedings*, vol. RMRS-P-41, 2006, pp. 213–220.

[28] *Pyrecast*, Pyregence, Jun. 2024. [Online]. Available: pyrecast.org.

[29] M. Pollack, R. Piansky, S. Gupta, A. Kody, and D. Molzahn, "Equitably allocating wildfire resilience investments for power grids: The curse of aggregation and vulnerability indices," 2024. arXiv: 2404.11520.

[30] C. Barrows, A. Bloom, A. Ehlen, *et al.*, "The IEEE reliability test system: A proposed 2019 update," *IEEE Transactions on Power Systems*, vol. 35, no. 1, pp. 119–127, 2020.

[31] S. Taylor, A. Rangarajan, N. Rhodes, J. Snodgrass, B. Lesieutre, and L. A. Roald, "California test system (CATS): A geographically accurate test system based on the California grid," *IEEE Transactions on Energy Markets, Policy and Regulation*, vol. 2, no. 1, pp. 107–118, 2024.

[32] Pacific Gas & Electric, *Public Safety Power Shutoffs*, 2024. [Online]. Available: https://www.pge.com/en/outages-and-safety/safety/community-wildfire-safety-program/public-safety-power-shutoffs.html.

[33] Southern California Edison, *Public Safety Power Shutoff*, 2024. [Online]. Available: https://www.sce.com/outage-center/outage-information/psps.

[34] San Diego Gas & Electric, *Public Safety Power Shutoffs*, 2024. [Online]. Available: https://www.sdge.com/wildfire-safety/public-safety-power-shutoffs.

[35] California Public Utilities Commission, *Utility PSPS Reports: Post-Event, Pre-Season and Post-Season*, 2024. [Online]. Available: https://www.cpuc.ca.gov/consumer-support/psps/utility-company-psps-reports-post-event-and-post-season.

[36] S. Pineda, J. M. Morales, Á. Porras, and C. Domínguez, "Tight big-Ms for optimal transmission switching," to appear in *Electric Power Systems Research,* presented at the *23rd Power Systems Computation Conference (PSCC)*, 2024.

[37] PACE, *Partnership for an Advanced Computing Environment (PACE)*.

[38] J. Bezanson, A. Edelman, S. Karpinski, and V. B. Shah, "Julia: A fresh approach to numerical computing," *SIAM Review*, vol. 59, no. 1, pp. 65–98, 2017.

[39] C. Coffrin, R. Bent, K. Sundar, Y. Ng, and M. Lubin, "PowerModels.jl: An Open-Source Framework for Exploring Power Flow Formulations," in *19th Power Systems Computation Conference (PSCC)*, 2018.

[40] Gurobi Optimization, LLC, *Gurobi Optimizer Reference Manual*, 2023. [Online]. Available: https://www.gurobi.com.